Refractive Index Functions of TiO 2 Nanoparticles

ARTICLE *in* THE JOURNAL OF PHYSICAL CHEMISTRY C · JANUARY 2013

Impact Factor: 4.77 · DOI: 10.1021/jp305303q

6 AUTHORS, INCLUDING:

Matti Alatalo
University of Oulu
86 PUBLICATIONS **1,493** CITATIONS
SEE PROFILE

Heikki Haario
Lappeenranta University of Technology
158 PUBLICATIONS **2,672** CITATIONS
SEE PROFILE

Erik Vartiainen
Lappeenranta University of Technology
70 PUBLICATIONS **989** CITATIONS
SEE PROFILE

Juho Jalava
ProfMath Oy
15 PUBLICATIONS **214** CITATIONS
SEE PROFILE

THE JOURNAL OF PHYSICAL CHEMISTRY C

Article

pubs.acs.org/JPCC

Refractive Index Functions of TiO_2 Nanoparticles

Sami Auvinen,*[,†] Matti Alatalo,[†] Heikki Haario,[†] Erik Vartiainen,[†] Juho-Pertti Jalava,[‡] and Ralf-Johan Lamminmäki[‡]

[†]Lappeenranta University of Technology, Faculty of Technology, Department of Mathematics and Physics, P.O. Box 20, FI-53851 Lappeenranta, Finland

[‡]Sachtleben Pigments Oy, Pori, Finland

ABSTRACT: Wavelength-dependent refractive index functions (RIFs) of $(TiO_2)_n$ nanoparticles (n = 2, 8, 18, 28, or 38) have been calculated by using the data from our previous density functional theory and time-dependent density functional theory photoabsorption calculations. The results show significant blueshifts and increased anisotropy in the RIFs of the nanoparticles, when compared to experimental bulk values. On the basis of the results, we conclude that, in the case of these ultrasmall particles, the RIFs may depend notably on the shape and structure of the cluster and on the other hand the fundamental absorption characteristics do not depend much on the rather limited cluster size range. The results also support the proposition that, in light-scattering measurements, one should not use the bulk RIF to model nanosize particles, at least in the case of TiO_2 particles. Our results shed some light into this computationally and experimentally very challenging area of nanoparticle properties.

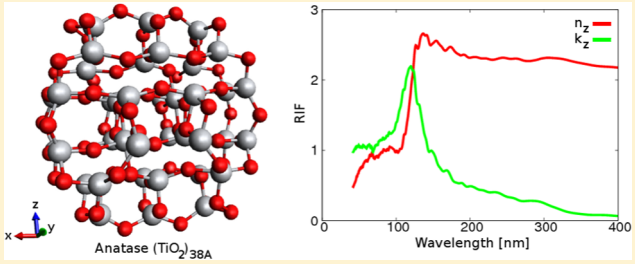

INTRODUCTION

Titanium dioxide is a wide band gap semiconductor that has gained a lot of interest due to its unique properties. TiO_2 is transparent in the visible region, while it absorbs strongly in the ultraviolet region. It is also photoactive, exhibits high surface reactivity with many chemical agents, and is nontoxic and cost-effective. Titanium dioxide is the most stable white pigment material because it is chemically highly resistant with other substances. In nature, TiO_2 occurs in three polymorphs: anatase, rutile, and brookite; the main source of industrially manufactured TiO_2 is ilmenite $FeTiO_3$.

In our previous publication,[1] we expressed the importance of submicrometer-size titanium dioxide pigment particles in many applications and described their production control by a recently developed light-scattering-based method, the turbidity spectrum method (TSM).[2] As it was pointed out,[1] we are now expanding the TSM to nanosize materials. By decreasing the particle size to the nanosize regime, many interesting applications become possible. This decrease changes the optical properties of TiO_2 remarkably from opaque to transparent in the visible range of the light spectrum and to an excellent UV-light blocker. These kinds of nanomaterials are widely used in many applications where visible-light transparency and UV shield are required such as sunscreens, wood lacquers, plastics, cosmetics, foods,[3,4] and photoelectronics.[5,6]

In the TSM, the particle size distribution (PSD) is determined from a turbidity spectrum measured from a diluted water solution by means of the T-matrix that is a rigorous light-scattering theory for nonspherical particles.[7,8] The TSM is now optimized for submicrometer size particles. The light-scattering computing requires the refractive index function (RIF) of the measured crystal material for all wavelengths used in the measurement. For submicrometer particles, the normal bulk values of RIFs are used. This is justified because, in the literature, we can find experiments proving that, for example, in the case of TiO_2 nanotubes, the diffuse reflectance UV−visible spectra match with bulk values when the nanotubes have diameters up from 5 nm and lengths around 500 nm.[9,10] However, there are studies indicating that the surface or the finite size of a very small particle can have an effect on the RIF especially at the UV wavelengths.[11] The TSM results are in accordance with these findings, and therefore, it is important to clarify this phenomenon. For that, we need to know how the RIF depends on the cluster size and shape.

As a first step, in our earlier paper,[1] electronic and spectral properties of small TiO_2 particles were studied using density functional theory (DFT) and time-dependent density functional theory (TDDFT) calculations. We had a focus on the shape changes of the calculated spectra, which can be related to changes in the RIF. Our results indicated that, in the case of small particles, their RIF can differ from the bulk values, and this has to be taken into account in the interpretation of light-scattering measurements.[1] In this paper, we report the RIFs that are calculated from the photoabsorption spectra for the previously optimized particle structures.[1] We have used two different sets of $(TiO_2)_n$ structures (n = 2, 8, 18, 28, or 38) along with the $(TiO_2)_2$ cluster. A similar study for bulk TiO_2

Received: May 31, 2012
Revised: January 30, 2013
Published: January 30, 2013

   dx.doi.org/10.1021/jp305303q | J. Phys. Chem. C 2013, 117, 3503−3512

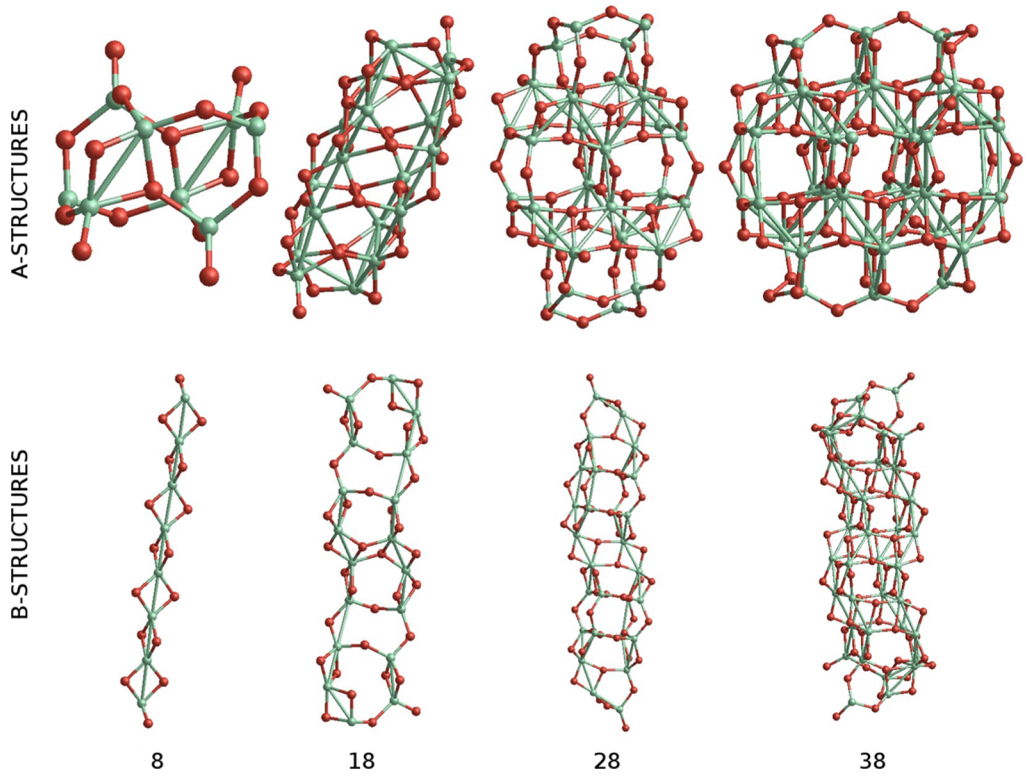

Figure 1. Relaxed A and B structures for $(TiO_2)_n$ clusters, n = 8, 18, 28, or 38. Titanium atoms are marked as green, and oxygen atoms are marked as red.

phases has been performed by Rocquefelte et al.[12] We also discuss the dielectric functions (DFs) of the particles.

THEORY

All DFT and TDDFT calculations for this study were performed by using the GPAW software,[13−16] which is a grid-based code using the projector-augmented wave (PAW) method.[17,18] The time-propagation TDDFT (TP-TDDFT) implementation in GPAW gives us the photoabsorption spectrum of the cluster as a function of the excitation energy of the photon, in the form of the dipole strength tensor,[16] which can be interpreted as a dipole strength function:[19]

$$S(\omega) = \frac{2m}{\pi e^2 \hbar}\omega \mathrm{Im}\ \alpha(\omega) \tag{1}$$

which has units of 1 per electronvolt. In eq 1, m is the mass of the electron, e is the charge of the electron, α is the polarizability of the system, and ω is the angular frequency. On the basis of eq 1, we can formulate the imaginary part of the polarizability to be

$$\mathrm{Im}\ \alpha(\omega) = \frac{\pi e^2 \hbar}{2m}\frac{S(\omega)}{\omega} \tag{2}$$

Because $E = \hbar\omega$, we can write eq 2 as

$$\mathrm{Im}\ \alpha(\omega) = \frac{\pi e^2 \hbar^2}{2m}\frac{S(\omega)}{E} \tag{3}$$

In eq 3, E is the excitation energy of the electrons, and when we use units $[S(\omega)] = 1/\mathrm{eV}$ and $[E] = \mathrm{eV}$, the term e^2 is canceled out in the equation.

The imaginary part of the DF can now be calculated based on eq 3 by using the equation for electronic polarization,[20] taking into consideration the fact that the electric field is local:

$$\varepsilon'' = \frac{N_v}{\varepsilon_0}\mathrm{Im}\ \alpha(\omega) \tag{4}$$

where N_v is the valence electron density of the system and ε_0 is the vacuum permittivity. The valence electron density of the system in eq 4 can be given by multiplying the number density of molecules $\mathcal{N}$[20] by the number of valence electrons per molecule $N_{v'}$:

$$N_v = \mathcal{N}N_{v'} = \frac{\rho}{M}AN_{v'} \tag{5}$$

where ρ and M are the density and molar mass of the substance, respectively, and A is the Avogadro number. Here, we have used the values ρ = 3.9 g/cm^3 and M = 79.88 g/mol for the anatase as given in refs 21 and 22. We have used the values for bulk anatase bacause the calculation of these values from the structures of the nanoparticles is not always straightforward. The number of valence electrons per molecule was set to be $N_{v'} = 2$, because all DFT calculations done here were spin paired, having two valence electrons in the highest occupied orbital. The calculated imaginary parts of the DFs were also scaled by dividing with the number of TiO_2 units in the cluster in order to remove the increase of the steady-state level as a function of increasing particle diameter.

The real parts of the DF were calculated by using the Kramers−Kronig relations,[23] and the complex RIFs were calculated from the DFs by using the well-known relations for nonmagnetic material:[24]

dx.doi.org/10.1021/jp305303q | J. Phys. Chem. C 2013, 117, 3503−3512

$$n = \frac{1}{\sqrt{2}}[(\varepsilon'^2 + \varepsilon''^2)^{1/2} + \varepsilon']^{1/2} \quad (6)$$

and

$$k = \frac{1}{\sqrt{2}}[(\varepsilon'^2 + \varepsilon''^2)^{1/2} - \varepsilon']^{1/2} \quad (7)$$

As a final step, the acquired RIFs were scaled by a shape-dependent scaling factor:

$$s_a = \left(\frac{l_{mean}}{l_a}\right)^{1/3} \quad (8)$$

where l_a is the length of the particle along the corresponding crystal axisand

$$l_{mean} = (l_x l_y l_z)^{1/3} \quad (9)$$

is the cubical effective mean dimension of the particle.

COMPUTATIONAL DETAILS

As described in our previous publication,[1] the selected cluster structures were relaxed by using a quasi-Newton minimizer, requiring all forces to be smaller than 0.05 eV/Å in the final sructures. In final relaxation runs, the width of the Fermi distribution was set to 0 eV giving us 0 K electronic temperature and integer occupation numbers. The used grid spacing was 0.17 Å, and the cell was set up with nonperiodic boundary conditions so that there was 7 Å of empty space surrounding the cluster. We used the Perdew–Burke–Ernzerhof (PBE) exchange correlation functional,[25] conjugate gradient method for the eigensolver, and all calculations were done using only the Γ-point. We did not use spin-polarized calculations, because the tests did not show any evidence about the spin-polarization in TiO_2 nanoparticles.

The photoabsorption spectra for the clusters were calculated by using the TP-TDDFT approach. We used a time step of 16.0 as with 1000 iterations and grid spacing of 0.3 Å. The kick parameter for initial perturbation of the wave functions was set to be 10^{-3}. The calculation cell was set up with nonperiodic boundary conditions with 10 Å of empty space surrounding the cluster. The spectra were calculated from the dipole moment files by using a Gaussian broadening of 0.1 eV.

RESULTS AND DISCUSSION

Bulk anatase TiO_2 has a tetragonal crystal structure with 12 atoms in the unit cell (four molecules/cell), and it belongs to the $I4_1/amd$ space group.[26] The experimental unit cell dimensions are $a = b = 3.784$ Å and $c = 9.515$ Å.[26] In our studies, we have used two different sets of TiO_2 structures along with the $(TiO_2)_2$ cluster: the structures, which were carved from the anatase bulk so that they would be as symmetric as possible in every direction still possessing as much bulklike structure as possible (labeled A), and the corresponding B structures, which were carved from the anatase bulk so that they would be longer in the z coordinate direction, forming a more needlelike structure. The relaxed A and B structures for $(TiO_2)_n$ clusters are presented in Figure 1. The dimensions of the structures are given in Table 1. The structures were cut so that x, y, and z coordinate axes correspond to the a, b,and c axes in the bulk anatase crystal. The structural analysis of the relaxed structures and their TDDFT photoabsorption spectra are presented in our previous publication.[1]

Table 1. Length of the Relaxed Structures in Each Coordinate Direction and Effective Mean Dimension of the Particle[a]

structure	l_x	l_y	l_z	l_{mean}
$(TiO_2)_2$	3.05	2.60	4.49	3.29
$(TiO_2)_{8A}$	6.04	5.39	6.78	6.04
$(TiO_2)_{18A}$	7.77	8.56	12.33	9.36
$(TiO_2)_{28A}$	8.52	9.91	15.29	10.89
$(TiO_2)_{38A}$	12.25	9.58	12.71	11.42
$(TiO_2)_{8B}$	4.67	3.26	21.43	6.89
$(TiO_2)_{18B}$	6.70	5.46	22.33	9.34
$(TiO_2)_{28B}$	6.66	5.26	29.18	10.07
$(TiO_2)_{38B}$	8.72	8.46	25.40	12.33

[a]All lengths are given in units of angstrom.

The RIFs for the A structures are presented in Figures 2–4, and the RIFs for the B structures are presented in Figures 5–7, where they are compared to the corresponding experimental data for bulk anatase reported by Jellison et al.[27] and Hosaka et al.[28] The reference data for bulk anatase was extracted from the articles by carefully digitizing and scaling. When we look at Figures 2,3,5, and 6, we see that, in the case of nanoparticles, the optical anisotropy is increased. The bulk anatase crystal structure is optically birefringent, and the RIFs of the a and b axes correspond to each other, while the c axis has a different RIF. This is due to the crystal structure of the ideal anatase bulk, which has an elongated unit cell in the c axis direction. In the case of the nanoparticles, the RIFs of the x and y directions differ from each other, although the basic form of the RIFs is quite similar. This is obviously due to changes in the crystal structure due to the finite size of the particles and thus an increased surface-to-bulk ratio, which was already observed previously in the analysis of the relaxation of the particle models.[1]

The maximum peak positions of the imaginary parts of the RIFs are collected in Table 2. According to Figures 2–7, the RIFs of the nanoparticles are generally significantly blueshifted when compared to the experimental values for bulk anatase. This was also predicted by the previous results on photoabsorption spectra.[1] Table 2 also contains the calculated blueshifts compared with experimental bulk data by Jellison et al.[27] and Hosaka et al.[28] When compared to the data set of Jellison et al.[27], the largest blueshift of the peak value of the imaginary part is 162 nm in k_z of the $(TiO_2)_{38A}$ cluster, and the average blueshift in the imaginary part of the RIF is 131 nm. When we compare the nanoparticle RIFs to the data set of Hosaka et al.[28], the largest blueshift of the peak value of the imaginary part is 141 nm in k_y of the $(TiO_2)_{18B}$ cluster, and the average blueshift in the imaginary part of the RIF is 101 nm. The negative values of $\Delta\lambda_{zmax2}$ in the case of $(TiO_2)_{8B}$, $(TiO_2)_{18B}$, and $(TiO_2)_{28B}$ indicate that the peak value is actually redshifted.

The refractive index data of Hosaka et al.[28] is measured for much smaller wavelengths than the data of Jellison et al.[27], so it is better to compare our nanoparticle RIFs to this data set. In the RIF data of Hosaka et al.,[28] one can notice small peaks in n_a at 120, 143, and 165 nm. The k_a has corresponding peaks at 120, 140, and 155 nm. The n_c has peaks at 124 and 159 nm, and k_c has peaks at 121 and 148 nm. As we can see in Figures 2–7 and Table 2, in the case of A structures, the maximum peak positions of the nanoparticle RIFs correspond quite well to these peaks at smaller wavelengths. In the case of B structures,

dx.doi.org/10.1021/jp305303q | J. Phys. Chem. C 2013, 117, 3503–3512

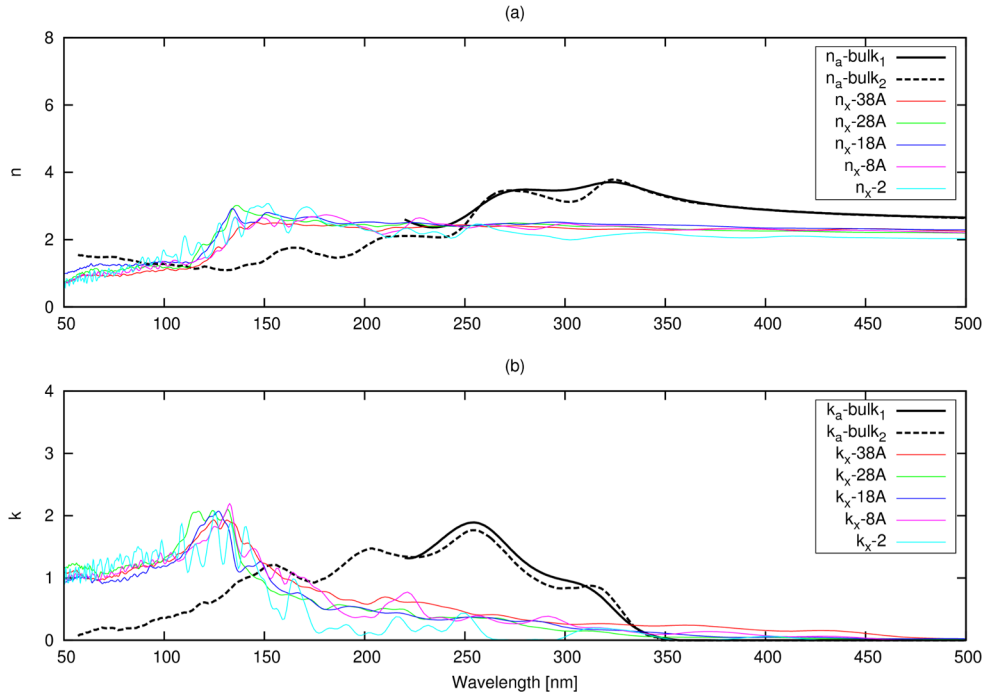

Figure 2. Calculated RIFs of A structures and the $(TiO_2)_2$ cluster in the *x* coordinate direction (*a* axis in the crystal) compared to the experimental values for anatase bulk (depicted as black). Experimental values for bulk anatase are from Jellison et al.[27] ($bulk_1$) and Hosaka et al.[28] ($bulk_2$).

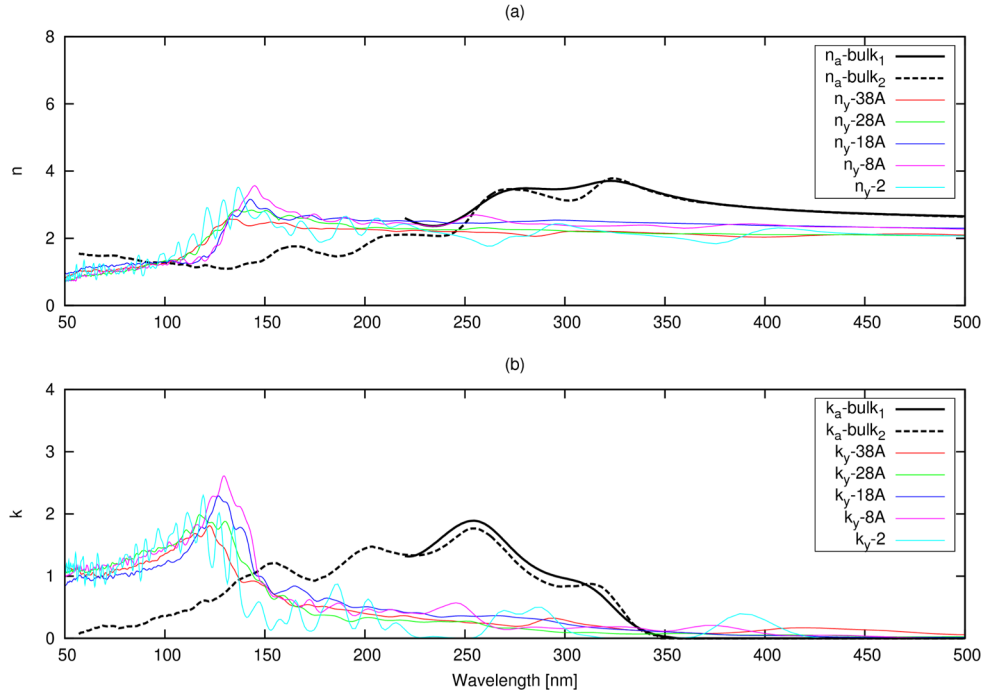

Figure 3. Calculated RIFs of A structures and the $(TiO_2)_2$ cluster in the *y* coordinate direction (*a* axis in the crystal) compared to the experimental values for anatase bulk (depicted as black). Experimental values for bulk anatase are from Jellison et al.[27] ($bulk_1$) and Hosaka et al.[28] ($bulk_2$).

the correspondence is quite good with n_a and k_a, but with n_c and k_c, the correspondence is not so good. On the basis of these findings, we can conclude that the weight of the RIFs moves toward shorter wavelengths when the particle size is decreased.

From Figures 2−7 and Table 2, we see that the shape and structure of the particle can have a more pronounced effect on the RIF than the actual particle size in the size area studied here. Generally, the RIFs of nanoparticles are clearly blue-shifted, but in this set of model structures, we do not see any size-dependent shift toward the bulk RIF. This is of course due to the relatively small particle size variation in the test set. What is also visible in Figures 2−7 is that the previously reported changes in the gap width of the nanoparticles do not seem to significantly affect the RIF of the particles. We have not used the Tauc Plot analysis[29] to resolve the band gaps from RIF data because the calculated band gaps were already reported in our previous article.[1] These results strengthen our previous conclusion that, in the case of ultrasmall particles, the spectra

dx.doi.org/10.1021/jp305303q | J. Phys. Chem. C 2013, 117, 3503−3512

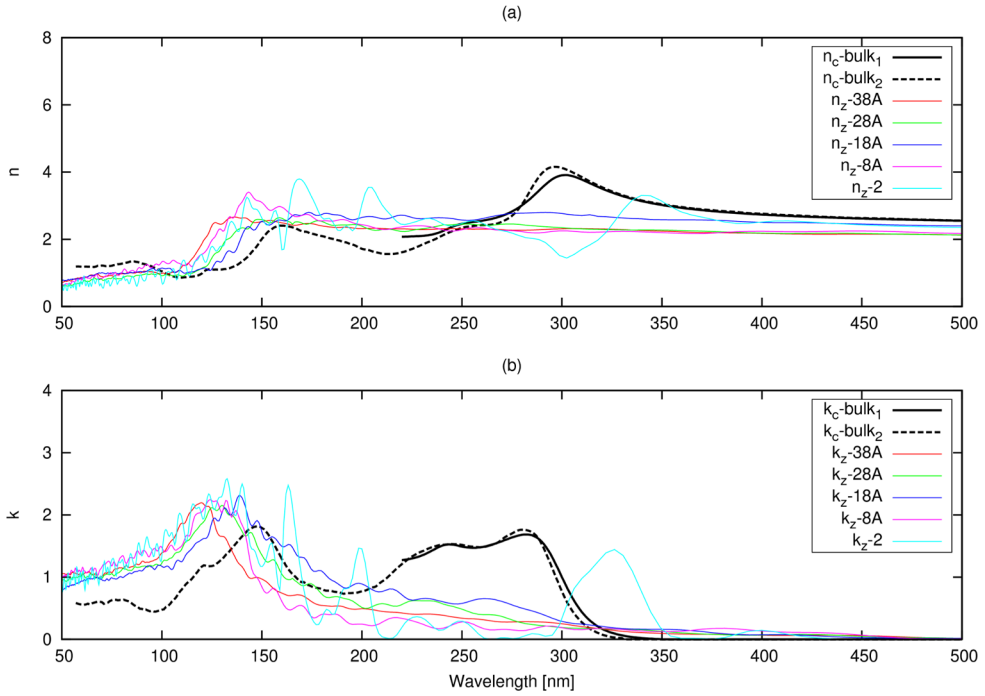

Figure 4. Calculated RIFs of A structures and the $(TiO_2)_2$ cluster in the z coordinate direction (c axis in the crystal) compared to the experimental values for anatase bulk (depicted as black). Experimental values for bulk anatase are from Jellison et al.[27] (bulk$_1$) and Hosaka et al.[28] (bulk$_2$).

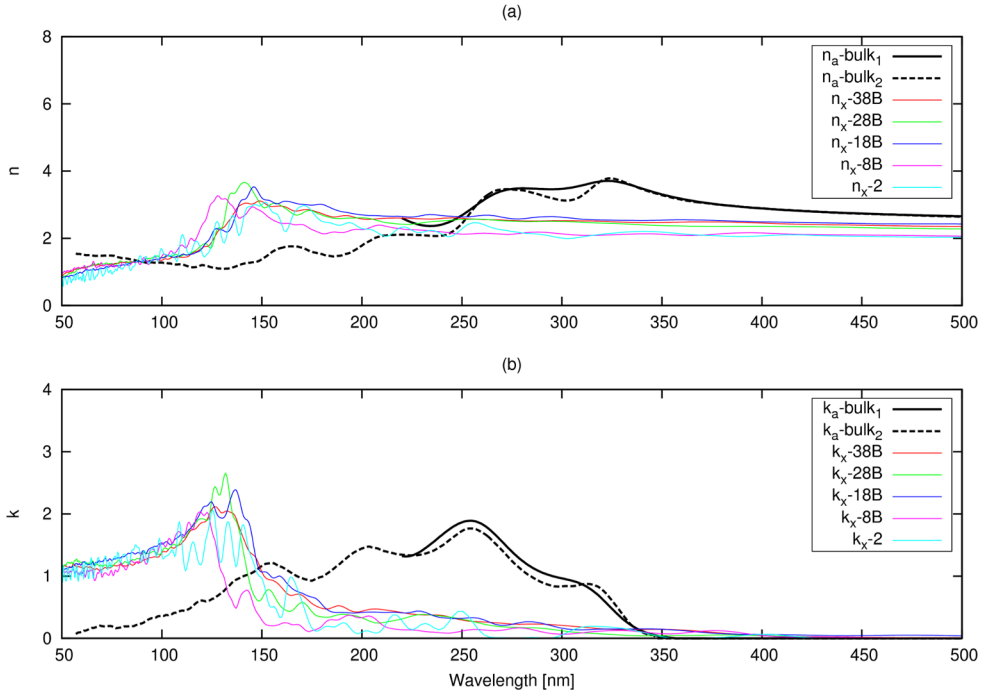

Figure 5. Calculated RIFs of B structures and the $(TiO_2)_2$ cluster in the x coordinate direction (a axis in the crystal) compared to the experimental values for anatase bulk (depicted as black). Experimental values for bulk anatase are from Jellison et al.[27] (bulk$_1$) and Hosaka et al.[28] (bulk$_2$).

and electronic structure may depend notably on the shape and structure of the cluster and on the other hand the fundamental absorption characteristics do not seem to depend so much on the size of the cluster at the particle sizes studied here.[1] It should be cleared out here that, with shape and structure, we refer to the actual shape of the cluster (prolonged or symmetric) and structural changes on the cluster surface (coordination and bonding due to different carving from bulk structure), as opposed to size, which is considered as a combination of dimensions and the amount of TiO_2 units in the cluster.

Besides the RIFs, the underlying dielectric properties are also important. The real and imaginary parts of DFs for clusters and the TiO_2 molecule are presented in Figures 8−11. In these figures, we have combined the DFs in perpendicular polarization directions (x and y) by calculating the average value for them. This way we can easily compare our cluster DFs with ones computed for bulk anatase by Asahi et al.[30] As we can see

dx.doi.org/10.1021/jp305303q | J. Phys. Chem. C 2013, 117, 3503−3512

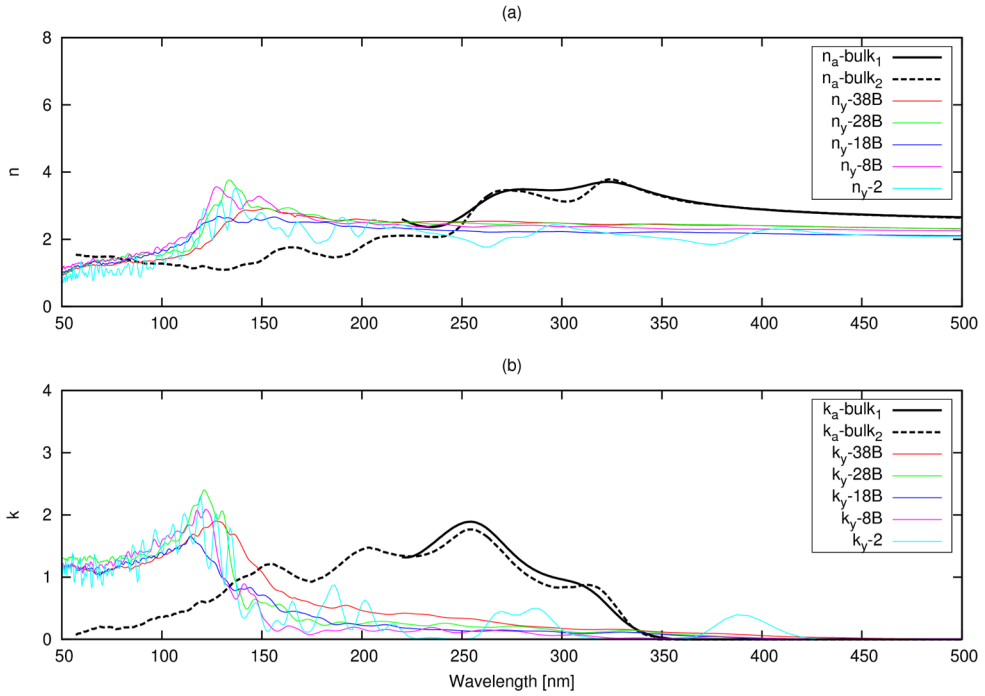

Figure 6. Calculated RIFs of B structures and the $(TiO_2)_2$ cluster in the *y* coordinate direction (*a* axis in the crystal) compared to the experimental values for anatase bulk (depicted as black). Experimental values for bulk anatase are from Jellison et al.[27] ($bulk_1$) and Hosaka et al.[28] ($bulk_2$).

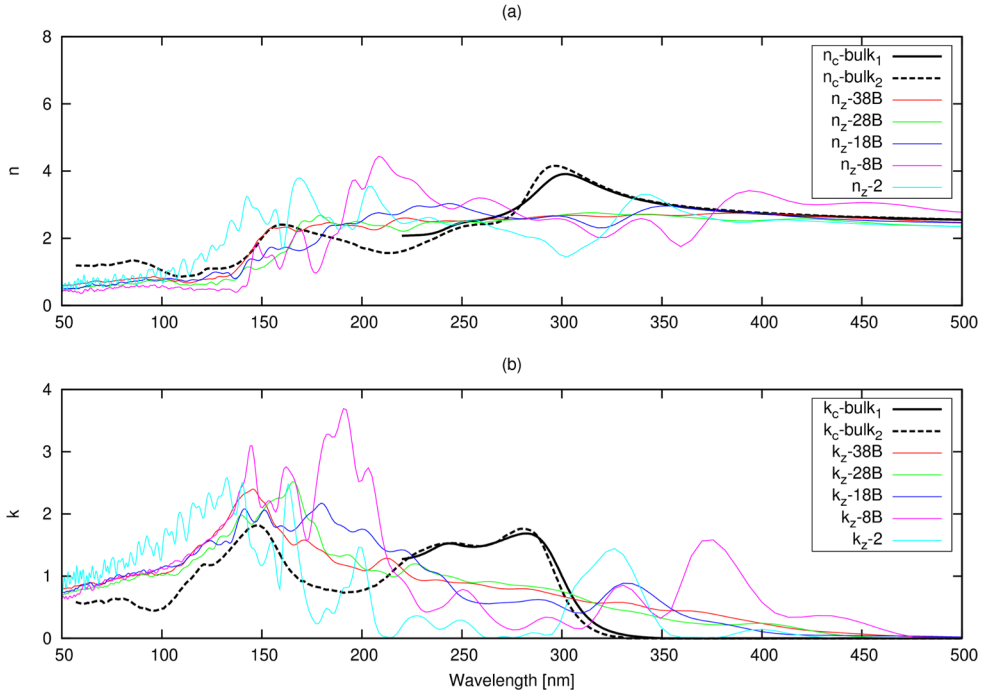

Figure 7. Calculated RIFs of B structures and the $(TiO_2)_2$ cluster in the *z* coordinate direction (*c* axis in the crystal) compared to the experimental values for anatase bulk (depicted as black). Experimental values for bulk anatase are from Jellison et al.[27] ($bulk_1$) and Hosaka et al.[28] ($bulk_2$).

in Figures 8−11 and from ref 30, the peak positions of the DFs for the clusters correspond well with peaks in computational bulk data and with the experimental data of Jellison et al.[27] and Hosaka al.,[28] especially in the *z* direction. The difference is that the clusters have much smaller DFs at the lower energy region around 3−7 eV. These peaks correspond to transitions from the valence bands to t_{2g} orbitals.[30]

As was already concluded with density of states (DOS) results in our previous publication,[1] the edges of the valence and conduction bands are more localized in the case of the clusters. The more localized the t_{2g} orbitals are, the lower the absorption peaks are at these energy levels when compared to transitions to e_g conduction bands at higher energy levels.[30] Also, the DOS at the edges of the band gap is relatively smaller than it is in the case of bulk structures.[1] This indicates that, when the size and shape-dependent formation of band structure reaches the point where t_{2g} orbitals become less localized, the clusters start to have more bulklike DFs and RIFs. As we

dx.doi.org/10.1021/jp305303q | J. Phys. Chem. C 2013, 117, 3503−3512

Table 2. Wavelengths (nm) of the Maximum Peak in the Imaginary Part of the RIF along Different Crystal Axes and Their Blueshifts Compared to the Experimental Values for Anatase Bulk[a]

				bulk$_1$			bulk$_2$		
structure	λ_{xmax}	λ_{ymax}	λ_{zmax}	$\Delta\lambda_{xmax1}$	$\Delta\lambda_{ymax1}$	$\Delta\lambda_{zmax1}$	$\Delta\lambda_{xmax2}$	$\Delta\lambda_{ymax2}$	$\Delta\lambda_{zmax2}$
$(TiO_2)_2$	125	119	133	129	135	149	130	136	15
$(TiO_2)_{8A}$	133	130	124	121	124	158	122	125	24
$(TiO_2)_{18A}$	127	127	139	127	127	143	128	128	9
$(TiO_2)_{28A}$	132	118	130	122	136	152	123	137	18
$(TiO_2)_{38A}$	125	122	120	129	132	162	130	133	28
$(TiO_2)_{8B}$	119	122	191	135	132	91	136	133	−43
$(TiO_2)_{18B}$	137	114	180	117	140	102	118	141	−32
$(TiO_2)_{28B}$	132	121	165	122	133	117	123	134	−17
$(TiO_2)_{38B}$	127	127	146	127	127	136	128	128	2
bulk$_1$ (expt)	254	254	282						
bulk$_2$ (expt)	255	255	148						

[a]The experimental data for bulk$_1$ is from Jellison et al.[27], and the experimental data for bulk$_2$ is from Hosaka et al.[28] The values $\Delta\lambda_{xmax1}$, $\Delta\lambda_{ymax1}$, and $\Delta\lambda_{zmax1}$ are the blueshifts relative to bulk$_1$ data, and $\Delta\lambda_{xmax2}$, $\Delta\lambda_{ymax2}$, and $\Delta\lambda_{zmax2}$ are the corresponding values relative to bulk$_2$ data.

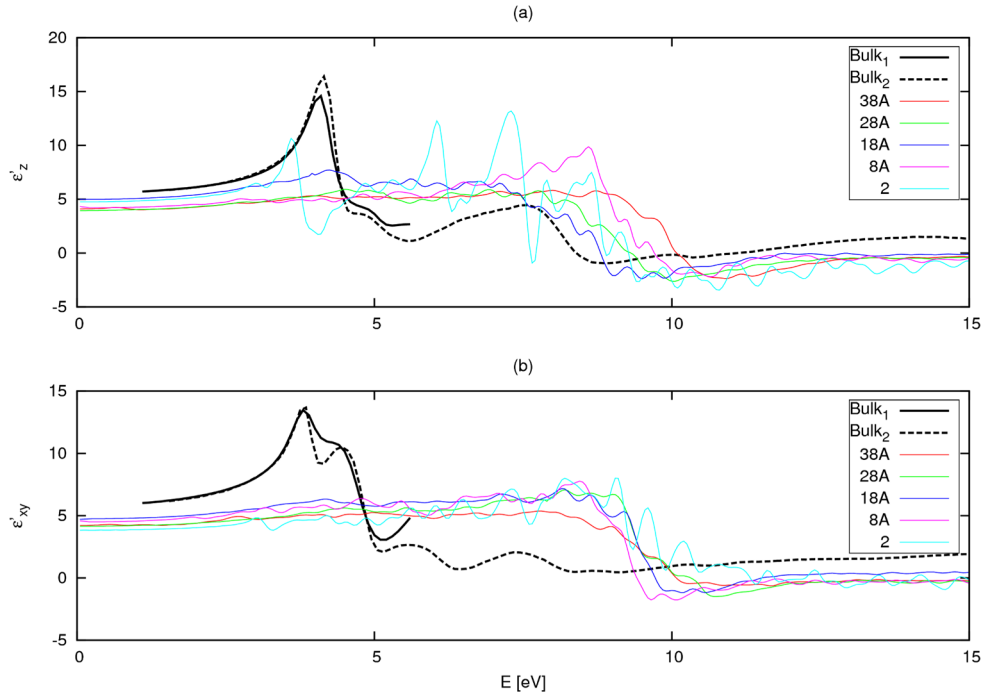

Figure 8. Calculated real parts of DFs for A structures and the $(TiO_2)_2$ cluster in the z coordinate direction (c axis in the crystal) (a), and in the xy coordinate direction (a axis in the crystal) (b). The calculated values are compared to the experimental values for anatase bulk (depicted as black). Experimental values for bulk anatase are from Jellison et al.[27] (bulk$_1$) and Hosaka et al.[28] (bulk$_2$).

already stated with the RIF results, the structure of the particle plays an important role in this band formation, as we can clearly see in the case of the $(TiO_2)_{8B}$ cluster. Figures 10 and 11 show that it has more absorption at the lower energy levels, and our earlier DOS results[1] confirm that, in the case of the $(TiO_2)_{8B}$ cluster, the localizaton of the band edges is lower than in the case of the other clusters (especially with t_{2g} orbitals).

All the results support the proposition that, in the TSM method, one should not use the bulk RIF to compute the PSD of nanosize particles. However, due to the limited size range achievable with first principles calculations, the exact size range of the particles where the transition toward the bulk RIF begins is still unknown. We will consider this in our future studies. The size of the largest particles studied here is already at the size range of industrial interest, and the RIFs of the largest particles can be used in parametrization when expanding the TSM to nanosize materials.

When interpreting the results, we should keep in mind that we are comparing computational results to experimental values, so the blueshifts reported here are not absolute and may contain small errors due to nature of the approximations used in DFT and TDDFT methods. In our calculations, we have used the PBE generalized gradient approximation (GGA) exchange correlation functional,[25] which provides many improvements opposed to original local density approximations. It is still generally known that the DFT and GGA approach tends to underestimate the fundamental band gap of semiconductors. This means that the actual blueshifts can be bigger than reported here. The underestimated gap in the imaginary part of the DF also affects the real part of the DF via

dx.doi.org/10.1021/jp305303q | J. Phys. Chem. C 2013, 117, 3503−3512

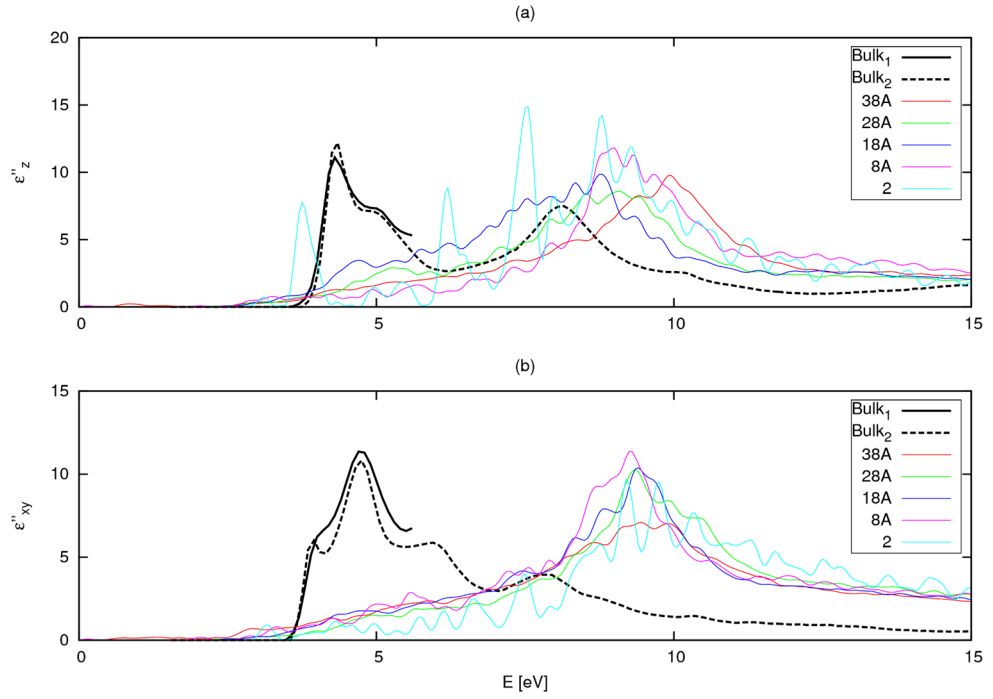

Figure 9. Calculated imaginary parts of DFs for A structures and the $(TiO_2)_2$ cluster in the *z* coordinate direction (*c* axis in the crystal) (a) and in the *xy* coordinate direction (*a* axis in the crystal) (b). The calculated values are compared to the experimental values for anatase bulk (depicted as black). Experimental values for bulk anatase are from Jellison et al.[27] ($bulk_1$) and Hosaka et al.[28] ($bulk_2$).

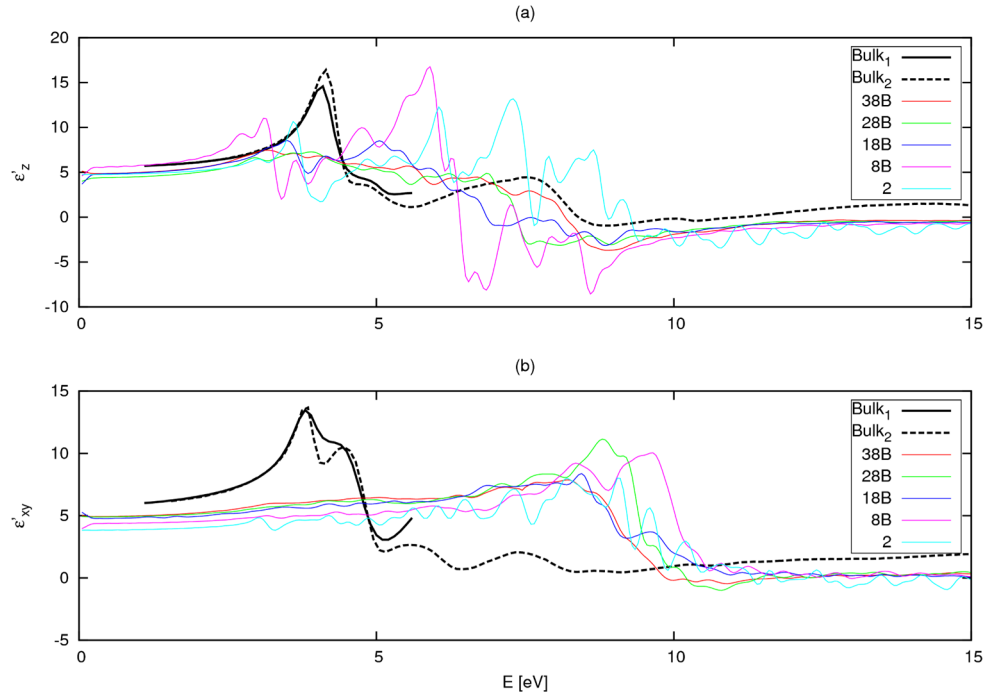

Figure 10. Calculated real parts of DFs for B structures and the $(TiO_2)_2$ cluster in the *z* coordinate direction (*c* axis in the crystal) (a) and in the *xy* coordinate direction (*a* axis in the crystal) (b). The calculated values are compared to the experimental values for anatase bulk (depicted as black). Experimental values for bulk anatase are from Jellison et al.[27] ($bulk_1$) and Hosaka et al.[28] ($bulk_2$).

Kramers–Kronig relations. However, the trends and general directions of the results are valid.

In the real-life applications (especially in the case of pigments), TiO_2 particles are also often in solutions containing water and other chemicals, such as sulfuric acid and possible trace elements,[31] possibly providing adatoms on the particle surfaces. Our current results do not take into account the effect of surface adatoms, which may change the photoabsorption of the particles due to the changes in the electronic structure.[32] We are currently working on effects of on-surface OH and SO_3 on the photoabsorption of TiO_2 nanoparticles, and these results will be published later.

Regarding the importance of exchange-correlation kernels, one should note that there are many ongoing research projects

dx.doi.org/10.1021/jp305303q | J. Phys. Chem. C 2013, 117, 3503–3512

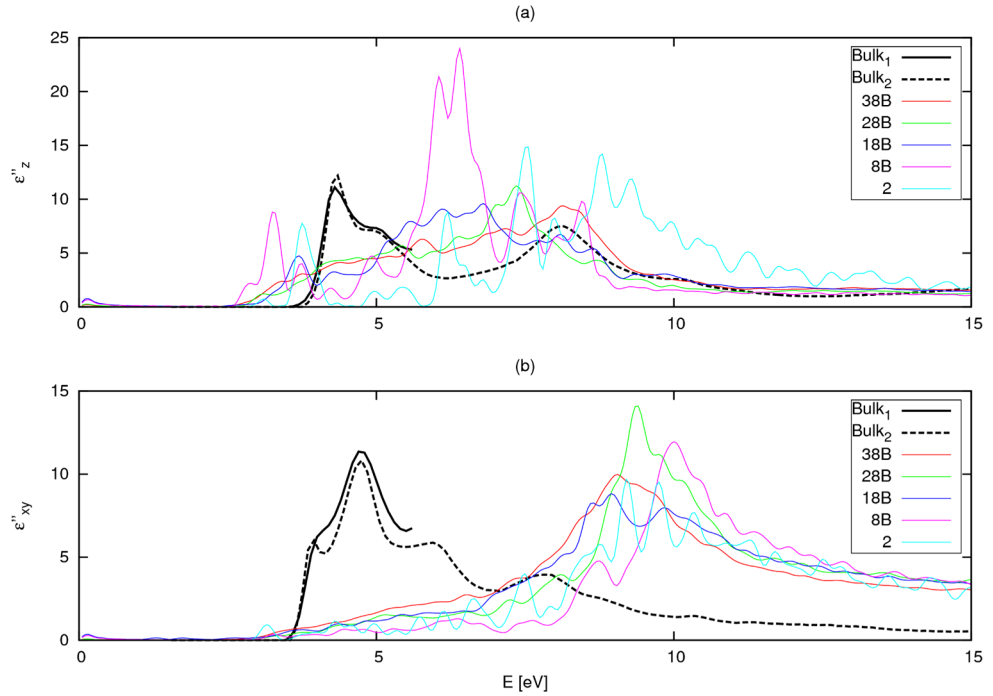

Figure 11. Calculated imaginary parts of DFs for B structures and the $(TiO_2)_2$ cluster in the *z* coordinate direction (*c* axis in the crystal) (a) and in the *xy* coordinate direction (*a* axis in the crystal) (b). The calculated values are compared to the experimental values for anatase bulk (depicted as black). Experimental values for bulk anatase are from Jellison et al.[27] ($bulk_1$) and Hosaka et al.[28] ($bulk_2$).

that aim to improve the earlier approximations. One example is a recent study of Gatti, who derived an exact form for the exchange-correlation kernel for time-dependent current density functional theory, allowing successful computation of electronic spectra of solids and nanosystems.[33]

In the case of the bulk semiconductors, there are studies suggesting that employing the Bethe–Salpeter equation (BSE)[34] can lead to improved optical results when compared to experimental values.[35] On the other hand, there are also studies indicating that, in the case of nanoparticles, the TDDFT approach can actually give more accurate results when compared to the BSE approach, as was found in the case of Si nanoparticles by Benedict et al.[36] Also the BSE implemantation in the GPAW software is restricted to periodic systems, leading to computationally demanding calculations in the case of nanoparticles. Thus, we have neglected the use of the BSE approach in our studies.

However, it should be stressed that the role of excitonic or electron–hole effects can have great importance in some cases of the nanostructures, underpinning the influence of structure and size. In 2008, Varsano et al. studied the optical saturation driven by exciton confinement in molecular chains by TDDFT methods and reported on the breakdown of commonly adopted approximations in anisotropic structures.[37] They concluded that the failure of simple local and semilocal functionals is due to the lack of memory effects, spatial ultranonlocality, and self-interaction corrections.[37] They also stated that simple approximations work better with small band gap systems, because these effects get smaller when the band gap is reduced.[37]

Our results reported in the present work shed some light into this computationally and experimentally very challenging area of nanoparticle properties and show that the use of the bulk RIF to model nanosize particles in light-scattering measurements is questionable, at least in the case of TiO_2 particles. The proper incorporation of excitonic and memory effects could still greatly further improve our current results, and other similar calculations, providing more information to fully clarify the optical behavior of nanoparticles.

CONCLUSIONS

RIFs of $(TiO_2)_n$ nanoparticles (n = 2, 8, 18, 28, or 38) were calculated based on the TDDFT data from our previous photoabsorption calculations.[1] The computational results were compared to the experimental ellipsometry data for the RIF of bulk anatase crystal reported earlier by Jellison et al.[27] and Hosaka et al.[28] The results show significant blueshifts (the averages are 131 nm in the imaginary part of the RIF when compared to data from Jellison et al.[27] and 101 nm when compared to data from Hosaka et al.[28]) and increased anisotropy in the RIFs of the nanoparticles. The results indicate that, in the case of ultrasmall TiO_2 particles, the structure of the particle may have a more pronounced effect on the RIF than the size of the particle and that the weight of the RIFs moves toward shorter wavelengths when the particle size is decreased. Current results show also that the anisotropy and blueshifts of the particle RIFs have to be taken into account in the TSM and light-scattering measurements of the small TiO_2 particles. However, the particle size on which the transformation of the particle RIF toward the bulk RIF starts still remains unknown. More studies are still needed to fully clarify this phenomenon.

AUTHOR INFORMATION

Corresponding Author

*E-mail: sami.auvinen@lut.fi.

Notes

The authors declare no competing financial interest.

■ ACKNOWLEDGMENTS

We want to acknowledge the Finnish Academy of Science and Letters, the Research Foundation of Lappeenranta University of Technology, and Sachtleben Pigments Oy, Pori, Finland, for funding this research. The computational resources were provided by CSC-Scientific Computing Ltd., Espoo, Finland.

■ REFERENCES

(1) Auvinen, S.; Alatalo, M.; Haario, H.; Jalava, J.-P.; Lamminmäki, R.-J. Size and Shape Dependence of the Electronic and Spectral Properties in TiO_2 Nanoparticles. *J. Phys. Chem. C* **2011**, *115*, 8484−8493.

(2) Jalava, J.-P.; Taavitsainen, V.-M.; Haario, H.; Lamberg, L. Determination of Crystal and Particle Size Distributions from Turbidity Spectrum of TiO_2 Pigment by Means of T-Matrix. *J. Quant. Spectrosc. Radiat. Transfer* **1998**, *60*, 399−409.

(3) Härkönen, R.; Aro, H.; Kujansivu, L. Optimisation of the Dispersing Process of Ultrafine Titanium Dioxide UV-TITAN M170: Effects on Sun Protection Factor and Transparency. *Cosmet. Toiletries Manuf. Worldwide* **2003**, 195−201.

(4) Härkönen, R.; Kujansivu, L. Ultrafine Titanium Dioxide: Effects on UV Protection. *Pers. Care Mag.* **2003**, *9*, 27−29.

(5) Karvinen, S.; Lamminmäki, R.-J. Preparation and Characterization of Mesoporous Visible-Light-Active Anatase. *Solid State Sci.* **2003**, *5*, 1159−1166.

(6) Salmi, M.; Tkachenko, N.; Lamminmäki, R.-J.; Karvinen, S.; Vehmanen, V.; Lemmetyinen, H. Femtosecond to Nanosecond Spectroscopy of Transition Metal-Doped TiO_2 Particles. *J. Photochem. Photobiol. A* **2005**, *175*, 8−14.

(7) Mishchenko, M.; Travis, L. D. Light Scattering by Polydispersions of Randomly Oriented Spheroid with Sizes Comparable to Wavelength of Observation. *Appl. Opt.* **1994**, *33*, 7206−7225.

(8) *Light Scattering by Nonspherical Particles. Theory, Measurements, and Applications*; Mishchenko, M., Hovenier, J. W., Travis, L. D., Eds.; Academic Press: London, 2000; pp 147−221.

(9) Tang, Z.-R.; Zhang, Y.; Xu, Y.-J. Tuning the Optical Property and Photocatalytic Performance of Titanate Nanotube toward Selective Oxidation of Alcohols under Ambient Conditions. *ACS Appl. Mater. Interfaces* **2012**, *4*, 1512−1520.

(10) Mukherjee, B.; Smith, Y. R.; Subramanian, V. R. CdSe Nanocrystal Assemblies on Anodized TiO_2 Nanotubes: Optical, Surface, and Photochemical Properties. *J. Phys. Chem. C* **2012**, *116*, 15175−15184.

(11) Bohren, C. F.; Huffman, D. R. *Absorption and Scattering of Light by Small Particles*, 1st ed.; Wiley: New York, 1983; pp 227−267.

(12) Rocquefelte, X.; Goubin, F.; Koo, H.-J.; Whangbo, M.-H.; Jobic, S. Investigation of the Origin of the Empirical Relationship between Refractive Index and Density on the Basis of First Principles Calculations for the Refractive Indices of Various TiO_2 Phases. *Inorg. Chem.* **2004**, *43*, 2246−2251.

(13) Mortensen, J. J.; Hansen, L. B.; Jacobsen, K. W. Real-Space Grid Implementation of the Projector Augmented Wave Method. *Phys. Rev. B* **2005**, *71*, 035109-1−035109-11.

(14) Enkovaara, J.; Rostgaard, C.; Mortensen, J. J.; Chen, J.; Dulak, M.; Ferrighi, L.; Gavnholt, J.; Glinsvad, C.; Haikola, V.; Hansen, H. A.; et al. Electronic Structure Calculations with GPAW: A Real-Space Implementation of the Projector Augmented-Wave Method. *J. Phys.: Condens. Mater.* **2010**, *22*, 253202-1−253202-24.

(15) Bahn, S. R.; Jacobsen, K. W. An Object-Oriented Scripting Interface to a Legacy Electronic Structure Code. *Comput. Sci. Eng.* **2002**, *4*, 56−66.

(16) Walter, M.; Häkkinen, H.; Lehtovaara, L.; Puska, M.; Enkovaara, J.; Rostgaard, C.; Mortensen, J. J. Time-Dependent Density-Functional Theory in the Projector Augmented-Wave Method. *J. Chem. Phys.* **2008**, *128*, 244101-1−244101-10.

(17) Blöchl, P. E. Projector Augmented-Wave Method. *Phys. Rev. B* **1994**, *50*, 17953−17979.

(18) Blöchl, P. E.; Först, C. J.; Schimpl, J. Projector Augmented Wave Method: Ab Initio Molecular Dynamics with Full Wave Functions. *Bull. Mater. Sci.* **2003**, *26*, 33−41.

(19) Martin, R. M. *Electronic Structure: Basic Theory and Practical Methods*, 1st ed.; Cambridge University Press: Cambridge, U.K., 2004; pp 406−417.

(20) Atkins, P. W.; Friedman, R. S. *Molecular Quantum Mechanics*, 3rd ed.; Oxford University Press: New York, 1997; pp 394−395.

(21) Clark, R. J. H. *The Chemistry of Titanium and Vanadium: An Introduction to the Chemistry of the Early Transition Elements*, 1st ed.; Elsevier: New York, 1968; pp 270−271.

(22) *CRC Handbook of Chemistry and Physics*, 68th ed.; Weast, R. C., Ed.; CRC Press: Boca Raton, FL, 1987; p B140.

(23) Lucarini, V.; Peiponen, K.-E.; Saarinen, J. J.; Vartiainen, E. M. *Kramers-Kronig Relations in Optical Materials Research*, 1st ed.; Springer: Berlin, Germany, 2005; pp 1−135.

(24) Bohren, C. F.; Huffman, D. R. *Absorption and Scattering of Light by Small Particles*, 1st ed.; Wiley: New York, 1983; pp 227−228.

(25) Perdew, J. P.; Burke, K.; Ernzerhof, M. Generalized Gradient Approximation Made Simple. *Phys. Rev. Lett.* **1996**, *77*, 3865−3868.

(26) Cromer, D. T.; Herrington, K. The Structures of Anatase and Rutile. *J. Am. Chem. Soc.* **1955**, *77*, 4708−4709.

(27) Jellison, G. E.; Boatner, L. A.; Budai, J. D.; Jeong, B.-S.; Norton, D. P. Spectroscopic Ellipsometry of Thin Film and Bulk Anatase (TiO_2). *J. Appl. Phys.* **2003**, *93*, 9537−9541.

(28) Hosaka, N.; Sekiya, T.; Satoko, C.; Kurita, S. Optical Properties of Single-Crystal Anatase TiO_2. *J. Phys. Soc. Jpn.* **1997**, *66*, 877−880.

(29) *Handbook of Ellipsometry*, 1st ed.; Tompkins, H. G., Irene, E. A., Eds.; William Andrew Publishing: New York, 2005; pp 145−146.

(30) Asahi, R.; Taga, Y.; Mannstadt, W.; Freeman, A. J. Electronic and Optical Properties of Anatase TiO_2. *Phys. Rev. B* **2000**, *61*, 7459−7465.

(31) Jalava, J.-P. Precipitation and Properties of TiO_2 Pigments in the Sulfate Process. 1. Preparation of the Liquor and Effects of Iron(II) in Isoviscous Liquor. *Ind. Eng. Chem. Res.* **1992**, *31*, 608−611.

(32) Iacomino, A.; Cantele, G.; Ninno, D.; Marri, I.; Ossicini, S. Structural, Electronic, and Surface Properties of Anatase TiO_2 Nanocrystals from First Principles. *Phys. Rev. B* **2008**, *78*, 075405−1−075405−11.

(33) Gatti, M. Design of Effective Kernels for Spectroscopy and Molecular Transport: Time-Dependent Current-Density-Functional Theory. *J. Chem. Phys.* **2011**, *134*, 084102−1−084102−5.

(34) Salpeter, E. E.; Bethe, H. A. A Relativistic Equation for Bound-State Problems. *Phys. Rev.* **1951**, *84*, 1232−1242.

(35) Yan, J.; Jacobsen, K. W.; Thygesen, K. S. Optical Properties of Bulk Semiconductors and Graphene/Boron Nitride: The Bethe-Salpeter Equation with Derivative Discontinuity-Corrected Density Functional Energies. *Phys. Rev. B* **2012**, *86*, 045208−1−045208−11.

(36) Benedict, L. X.; Puzder, A.; Williamson, A. J.; Grossman, J. C.; Galli, G.; Klepeis, J. E.; Raty, J.-Y.; Pankratov, O. Calculation of Optical Absorption Spectra of Hydrogenated Si Clusters: Bethe-Salpeter Equation Versus Time-Dependent Local-Density Approximation. *Phys. Rev. B* **2003**, *68*, 085310−1−085310−8.

(37) Varsano, D.; Marini, A.; Rubio, A. Optical Saturation Driven by Exciton Confinement in Molecular Chains: A Time-Dependent Density-Functional Theory Approach. *Phys. Rev. Lett.* **2008**, *101*, 133002−1−133002−4.